Mechanisms of irreversible aquaporin-10 inhibition by organogold compounds studied by combined biophysical methods and atomistic simulations

Catarina Pimpão [1,‡], Darren Wragg [2,‡], Riccardo Bonsignore [2], Brech Aikman [2,3], Per Amstrup Pedersen [4], Stefano Leoni [3], Graça Soveral [1,*] and Angela Casini [2,*]

[1]Research Institute for Medicines (iMed.ULisboa), Faculty of Pharmacy, Universidade de Lisboa, 1649-003 Lisboa, Portugal, [2] Department of Chemistry, Technical University of Munich, 85747 Garching bei München, Germany, [3] School of Chemistry, Cardiff University, Main Building, Park Place, Cardiff CF10 3AT, UK and
[4]Department of Biology, University of Copenhagen, Universitetsparken 13, DK-2100 Copenhagen OE, Denmark

[*] **Correspondence**: Prof. A. Casini: Department of Chemistry, Technical University of Munich, Lichtenbergstr. 4, 85748 Garching b. München, Germany, Ph:+49 (89) 289 - 13831; Prof. G. Soveral: Research Institute for Medicines (iMed.ULisboa), Faculty of Pharmacy, Universidade de Lisboa, 1649-003 Lisboa, Portugal. E-mails: angela.casini@tum.de; gsoveral@ff.ulisboa.pt

[‡]Shared first authors

Abstract

The inhibition of glycerol permeation via human aquaporin-10 (hAQP10) by organometallic gold complexes has been studied by stopped-flow fluorescence spectroscopy, and its mechanism has been described using molecular modelling and atomistic simulations. The most effective hAQP10 inhibitors are cyclometalated Au(III) C^N compounds known to efficiently react with cysteine residues leading to the formation of irreversible C–S bonds. Functional assays also demonstrate the irreversibility of the binding to hAQP10 by the organometallic complexes. The obtained computational results by metadynamics show that the local arylation of Cys209 in hAQP10 by one of the gold inhibitors is mapped into a global change of the overall free energy of glycerol translocation across the channel. Our study further pinpoints the need to understand the mechanism of glycerol and small molecule permeation as a combination of local structural motifs and global pore conformational changes, which are taking place on the scale of the translocation process and whose study, therefore, require sophisticated molecular dynamics strategies.

Keywords: aquaglyceroporin, glycerol transport, water, gold compounds, irreversible inhibitors, metadynamics

Graphical abstract

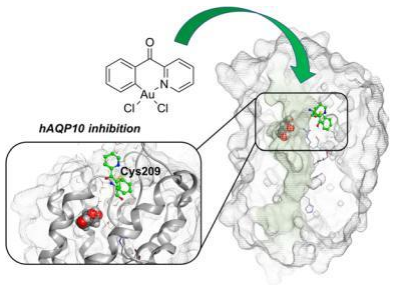

A new family of AQP-10 gold inhibitors has been identified and their mechanism of irreversible inhibition by cysteine arylation was studied by in vitro and in silico methods.

Introduction

Aquaporins (AQPs) are membrane-embedded protein channels that facilitate transmembrane diffusion of water and a few small neutral solutes in response to osmotic or solute gradients[1]. Humans express 13 AQPs (AQP0-12) in various cell types and body tissues and all isoforms are involved in essential physiological functions, such as urine concentration in the kidney, skin hydration, gland fluid secretion, brain fluid homeostasis, cell migration and proliferation, and adipocyte metabolism[1] While classical or orthodox AQPs are mainly water channels, the aquaglyceroporin subfamily comprises four isoforms (AQP3, AQP7, AQP9, AQP10) that are permeable to both water and glycerol. Aquaglyceroporins contribute to the body energy homeostasis and are involved in a number of metabolic and inflammatory disorders[2–4] fostering drug development opportunities for aquaporin-based therapies.[5]

AQP10 is expressed in human small intestine[6,7] and reported to be downregulated in inflammatory intestinal disorders such as celiac disease.[8] AQP10 is also expressed in human adipocytes where AQP7 is the main glycerol channel and has been suggested as an alternative pathway for glycerol efflux from the adipose tissue during lipolysis, preventing from fat accumulation and obesity.[9,10]

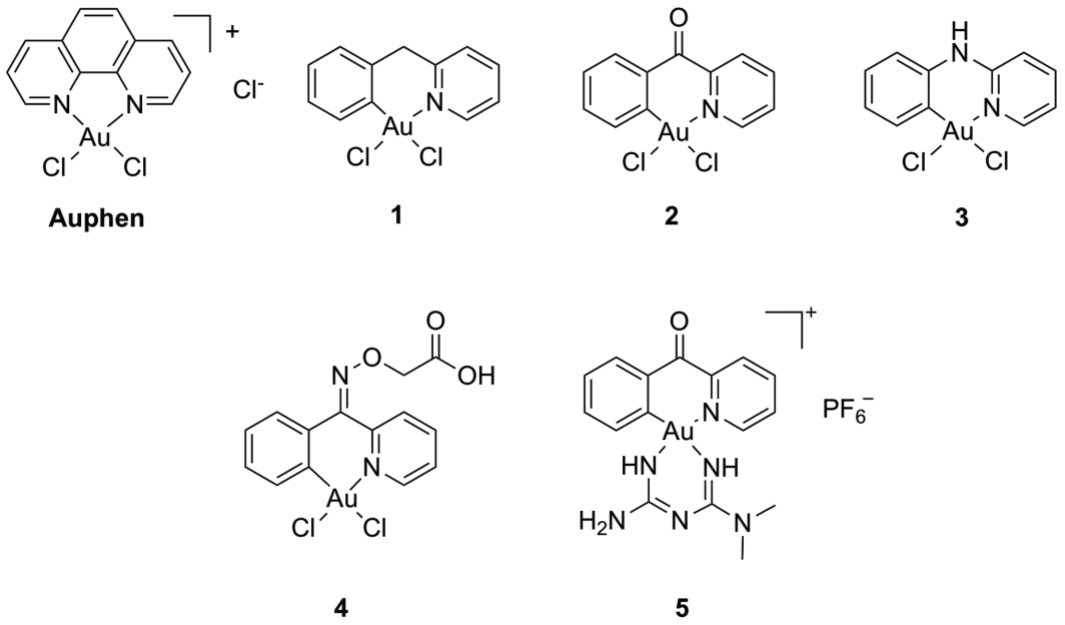

Fig. 1 Structures of the Au(III) compound Auphen and of cyclometalated Au(III) C^N complexes **1–5**.

The functional unit of human AQPs is a tetramer with each monomer providing an independent channel. The latter consists of an extracellular and intracellular vestibule connected by an extended narrow pore. Various structural studies revealed water molecules passing through the AQPs channel in a single file, ori-enting themselves along the local electrical field.[11] Two main con-striction sites have been identified within the channel to be re-sponsible for substrate selectivity: (i) the aromatic/arginine (ar/R) selectivity filter (SF), in proximity to the extracellular pore en-trance (EP), forms the narrowest part of the pore, and (ii) two conserved Asn-Pro-Ala motifs (NPA) in the middle of the channel, where the positive N-terminal ends of two half helices meet.[11–13] The formed helix dipole moment in this region adds to these pos-itive ends, creating an electrostatic barrier that prevents passage of positively charged ions through the pore.[14] The two asparagines in the NPA region act as hydrogen donors to the oxygen atoms of permeating substrates. In addition, water that enters this region is re-oriented by the dipoles of the emanating half helices, such that hydrogen bonds between neighbouring water molecules in the chain are disrupted. In the case of human AQP10, the con-served residues are Arg217 and Ile211 for the ar/R region, and Asn82 and Ans214 for the NPA motif, respectively.[10] A third con-striction region, mechanistically unique to AQP10, is located in the intracellular side of the pore (IP), whereby the configuration and interaction of Phe85 with His80 and Arg94 create a narrowing of the pore size to 0.9 Å, which at pH 7.4 prevents the passage of glycerol, while still allowing for water flux.[10] This region has pre-viously been shown to be responsible for the hAQP10 pH gating mechanism involving the double protonation of the highly con-served histidine (His80).[10]

In the past years, we have devoted our investigation to the design of AQPs selective inhibitors, specifically gold-based com-pounds with bidentate N-donor ligands.[15,16] For example, the Au(III) compound [Au(phen)Cl_2]Cl (phen = 1,10-phenanthroline) (Auphen, Fig. 1) has been reported to be a selective and potent inhibitor of glycerol permeation by human AQP3, while having no inhibitory effect on water permeability mediated by AQP1.[17] Further studies also demonstrated moderate inhibitory properties of Auphen towards human AQP7.[18,19] A combination of *in silico* approaches and site-directed mutagenesis studies revealed that the mechanism of inhibition involves binding of the Au(III) centre to the thiol moiety of a selected Cys residue in AQP3 (Cys40).[17,20,21] Remarkably, molecular dynamics (MD) studies con-ducted on Au(III) complexes–AQP3 adducts showed that protein conformational changes, resulting from metal binding to Cys40, are mostly responsible for the observed inhibition of water and glycerol permeation.[22]

To the best of our knowledge, no inhibitors of human AQP10 have been reported so far.[15,23] Therefore, we investi-gated the effects of a small library of gold compounds on glycerol and water permeation by hAQP10. These include cy-clometalated Au(III) complexes with bidentate C^N ligands— [Au($C^{CH2}N$)Cl_2] (**1**, $C^{CH2}N$ = 2-benzylpyridine),[24] [Au($C^{CO}N$)Cl_2] (**2**, $C^{CO}N$ = 2-benzoylpyridine),[25] [Au($C^{NH}N$)Cl_2] (**3**, $C^{NH}N$ = *N*-phenylpyridine-2-amine),[26] [Au($C^{NOx}N$)Cl_2] (**4**, $C^{NOx}N$ = 2-(phenyl-(2-pyridinylmethylene)aminoxy acetic acid))[27] and the cationic [Au($C^{CO}N$)met]PF_6 (**5**, met = metformin)[28] (Fig. 1). Compound **1** was previously shown to be a moderate inhibitor of human AQP3.[22] For the purpose of identifying inhibitors of hAQP10, the protein was expressed in an optimized yeast expression model,[19,29,30] consisting of a *Saccharomyces cerevisiae* strain de-pleted from endogenous aquaporins and transformed with a plas-mid encoding hAQP10.[10] Permeability assays using stopped-flow fluorescence spectroscopy confirmed the glycerol channelling fea-ture of hAQP10 and were used to evaluate the inhibitory effect of the selected gold-based compounds on hAQP10 glycerol perme-ability, as well as to address the mechanism of binding.

The compounds were selected amongst a family of organometallic derivatives, featuring a direct Au–carbon bond, being endowed with increased stability in aqueous environment relative to the benchmark inhibitor Auphen, as well as featuring a peculiar reactivity with cysteine residues. Specifically, it has been demonstrated that, following AuC^N-Cys adduct formation, the reaction of complexes **1–3** with peptides proceeds towards cysteine arylation (Scheme 1).[31] Combined mass spectrometry and density functional theory (DFT) calculations showed that

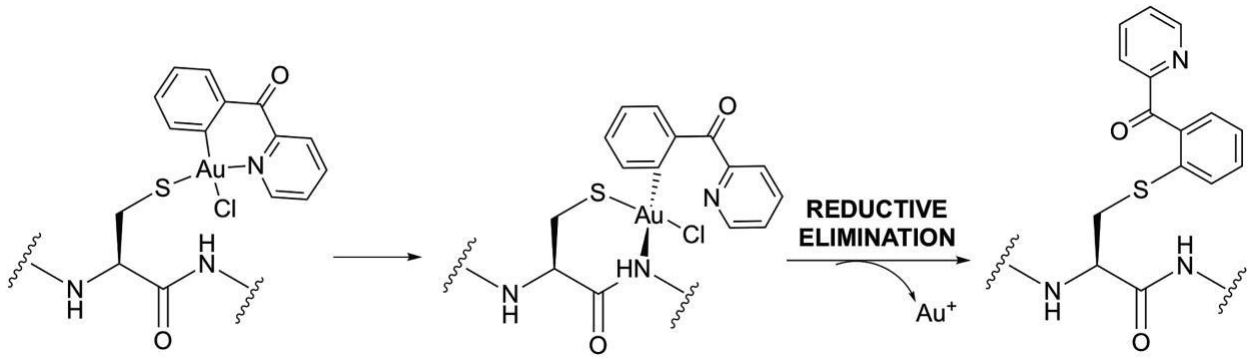

Scheme 1 Proposed mechanism of cysteine arylation by Au(III) C^CON complex **2** *via* reductive elimination.[31]

formation of the C^N-peptide adduct is templated by the Au(III) centre facilitating the C–S cross-coupling reaction *via* reductive elimination.[31,32] Thus, a general reaction mechanism for cysteine arylation was proposed whereby a cysteinate residue binds *trans* to the N of the C^N ligand, while a second peptidic residue X coordinates to Au(III), favouring bond breakage between the nitrogen and the metal to achieve the [Au(C^N)(Cys)XCl] species (Scheme 1).[33] Formation of the latter intermediate is crucial for promoting the observed C–S cross-coupling.

In order to investigate the mechanisms of hAQP10 inhibition by cyclometalated Au(III) compounds, we applied atomistic simu-lations. Specifically, we used metadynamics on selected reaction coordinates, so-called collective variables (CVs),[34] along which the free energy of complex molecular systems can be integrated. This technique allows acceleration of conformational transitions between metastable states, markedly broadening the scope of straightforward MD simulations. This approach has previously been successfully applied to calculate the free-energy surface (FES) for the interactions of substrates/drugs with biomolecules, including DNA secondary structures.[35] We recently applied the same method to the study of glycerol and hydrogen perox-ide permeation via human AQP3.[36,37] Notably, metadynamics showed that water nanoconfinement within aquaporin channels results into steady bidirectional water movement along single file chains.[36] Such intrinsic water dynamics is crucial for substrate molecule solvation and transport in both directions of the AQP3 channel. Here, we used this method to study the effects of Cys arylation by compound **2** on both glycerol and water flux across human AQP10.

Results and discussion

hAQP10 inhibition studies by stopped-flow fluorescence spectroscopy

The benchmark AQP3 inhibitor Auphen and five cyclometalated Au(III) complexes **1–5** (Fig. 1) were synthesized following previ-ously reported procedures.[24–28,38] hAQP10 activity was assessed by stopped-flow fluorescence of yeast cells depleted of endogenous aquaporins (aqy-null) and transformed with either the empty ex-pression plasmid or the plasmid encoding hAQP10. At pH 5.0, the measured glycerol permeability (P_{gly}) for hAQP10-expressing yeast cells ($(27.30 \pm 9.62) \times 10^{-8}$ cm s^{-1}) was 270-fold higher than for the empty vector ($(0.10 \pm 0.001) \times 10^{-8}$ cm s^{-1}), confirming the func-tionality of hAQP10 in yeast transformants (Fig. 2A). It should be noted that in yeast and in some mammalian cells devoid of glyc-erol channels/transporters, glycerol permeation by passive diffu-sion is not detectable.[39,40] The water permeability (P_f) at pH 5.0 was slightly higher for hAQP10-expressing yeast cells ($(4.25 \pm 0.17) \times 10^{-4}$ cm s^{-1}) than the empty vector ($(3.74 \pm 0.15) \times 10^{-4}$ cm s^{-1}) (Fig. 2B), although the difference is not statistically signifi-cant. Pre-treatment of hAQP10-expressing cells with Auphen (10 μM for 30 min) caused only a slight decrease of P_f (ca. 10%).

To assess the inhibitory effect of gold-based compounds on hAQP10-mediated glycerol permeability, yeast cells were incu-bated with the cyclometalated Au(III) complexes **1–5** and Auphen (10 μM for 30 min) prior to performing permeability assays. Fig-ure 2C depicts representative traces of stopped-flow fluorescence spectroscopy experiments, illustrating the rapid shrinking and subsequent re-swelling responses in hAQP10 cells before (control) and after treatment with compound **2** (10 μM, 30 min). As shown in Fig. 2D, Auphen was the most potent inhibitor of glycerol per-meation, up to ca. 100% inhibition at the tested concentration. Amongst the cyclometalated Au(III) complexes, the strongest in-hibitory effect was observed for compounds **4**, **2**, and **1** (81%, 74%, and 70%, respectively), followed by compounds **3** and **5** (47% and 33%, respectively) that revealed less potency in inhibiting hAQP10 ability to transport glycerol. It is worth mentioning that complex **1** appears more active as inhibitor of AQP10 than of AQP3 (IC_{50} ca. 50 μM in human red blood cells), although care should be applied when comparing different cellular systems.[22] Similarly, complexes **2** and **3** induced the same reduction of glycerol perme-ation via AQP3 only when applied at 50 μM concentration (data not shown).

Complexes **1–3** can, following AuC^N-Cys adduct formation, re-act with peptides to enable cysteine arylation. In particular, com-pound **2** was described as the most prone to reductive elimination and cysteine arylation, followed by **1** and **3**, respectively,[31] in line with the observed inhibitory effects. Compound **5** is also likely to give Cys arylation; however, the presence of the metformin biden-tate ligand may prevent ligand exchange reactions at the metal centre and subsequent Au(III) binding to thiol groups. Further-more, the overall compound's positive charge may prevent its in-teraction with the EP region.

To further investigate the mechanism of binding to hAQP10, we assessed the reversibility of inhibition by **2** following estab-lished protocols.[22] Thus, cells were pre-treated with 10 μM of com-pound **2** for 30 min and were subsequently washed with either isotonic buffer or with β-mercaptoethanol (βME) (100 μM) before conducting the permeability assays. In parallel, the same exper-iment was performed for the coordination complex Auphen. As depicted in Fig. 2E, washing the cells with isotonic buffer or with βME had no effect in the recovery of hAQP10 glycerol permeability inhibited by compound **2**. Regarding Auphen, a partial recovery of hAQP10 glycerol permeability was obtained by washing the cells with either isotonic buffer or with βME. Considering that βME, which reacts with cysteine sulfhydryl groups, failed to compete

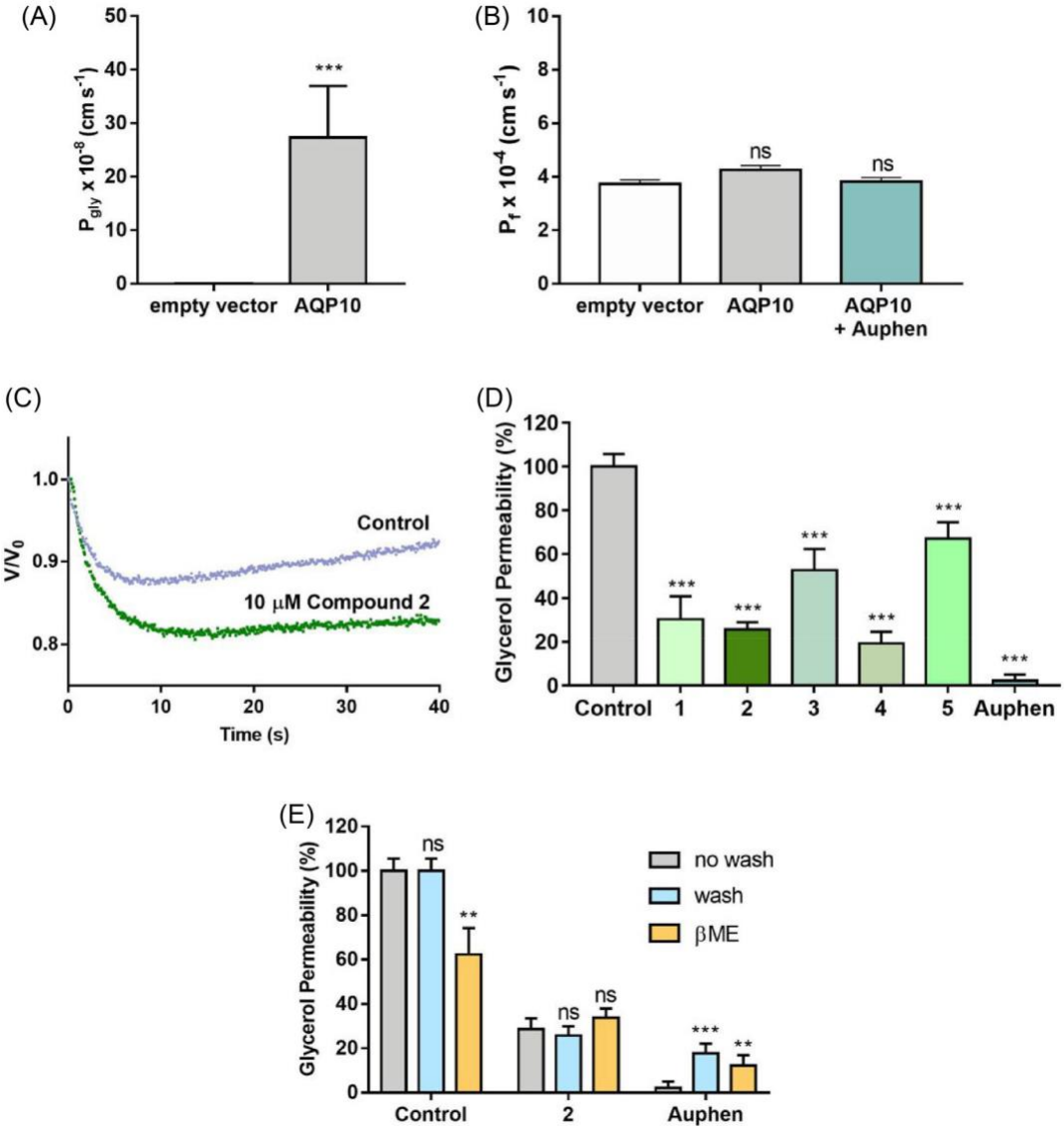

Fig. 2 (A) Glycerol permeability (P_{gly}) and (B) water permeability (P_f) of yeast cells transformed with the empty vector or expressing hAQP10 at pH 5.0. Water permeability inhibition by Auphen (10 μM, 30 min) is also shown. (C) Representative stopped-flow fluorescence spectroscopy experiments for glycerol permeability, illustrating the rapid change in relative cell volume responses of hAQP10-expressing yeast cells, non-treated (control) or treated with compound **2** (10 μM, 30 min). (D) Glycerol permeability of hAQP10-expressing yeast cells non-treated (control) or treated with organogold compounds **1**–**5** or Auphen (10 μM for 30 min). (E) Inhibition of glycerol permeability of cells treated with compound **2** or Auphen (10 μM, 30 min), and permeability recovery after washing with isotonic buffer or by *β*-mercaptoethanol (100 μM for 30 min). Data are mean ± SD of three independent experiments. ns, non-significant; ** $p < 0.01$; *** $p < 0.001$, treated vs non-treated cells.

with compound **2** for hAQP10 binding, it is possible that com-pound **2** establishes an irreversible covalent bond to an AQP10-cysteine residue, likely to arise from cysteine arylation. The same effect was not verified in cells pre-treated with Auphen, in line with the more reversible nature of the direct Au-Cys coordinative bond.[22,41]

hAQP10 molecular modelling and metadynamics simulations

Afterwards, a model system of membrane-embedded human hAQP10 was built from the available crystal structure (PDB ID 6F7H).[10] At physiological conditions, hAQP10 is functional at pH 5, therefore the relevant residues were protonated using the PDB2PQR server,[42] resulting in the protonation of His80. The proto-nated porin tetramer was then embedded into a POPE lipid bilayer (203 molecules) to simulate the cell membrane, following previously reported procedures.[19,22] As a second step, another hAQP10 model was built, featuring the $C^{CO}N$ ligand from compound **2** co-valently bound to the sulphur of Cys209 (Fig. 3), the latter being the only Cys accessible to the compound from the extracellular side and present in the channel. Afterwards, glycerol molecules (20 in each system) were added to study the mechanism of solute passage through the pore in each system and to determine the effects of the covalently bound $C^{CO}N$ ligand on glycerol conduc-tance.

In straightforward MD simulations, the passage of glycerol has low probability of being observed through a spontaneous system fluctuation. Therefore, to increase the probability of such a *rare event* within a simulation, metadynamics was used to encourage the glycerol substrate to explore the whole system, from which a detailed FES can be reconstructed. All glycerol molecules were in-dividually biased, using a separate plumed control file,[27] in which

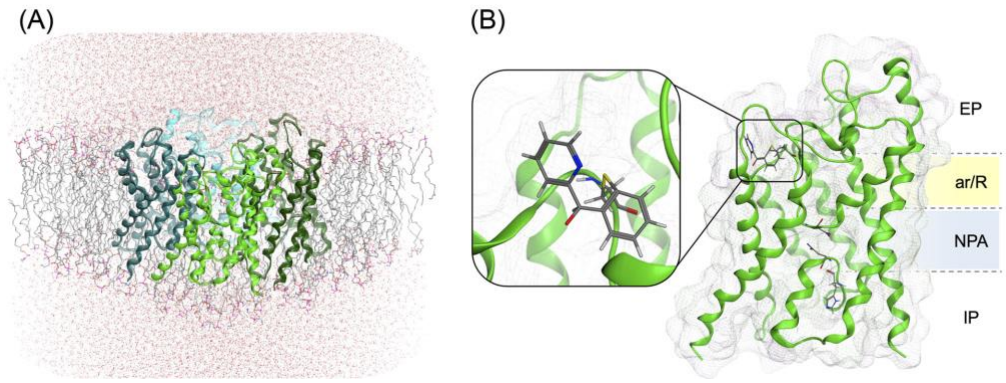

Fig. 3 (A) Crystal structure of human AQP10 (PDB-ID 6F7H)[10] tetramer embedded in the lipid bilayer. (B) hAQP10 monomer side view showing position of the NPA motif and the highly conserved His80, with a zoom showing the position of the covalently bound $C^{CO}N$ ligand to Cys209. Figure generated using MOE software.[43]

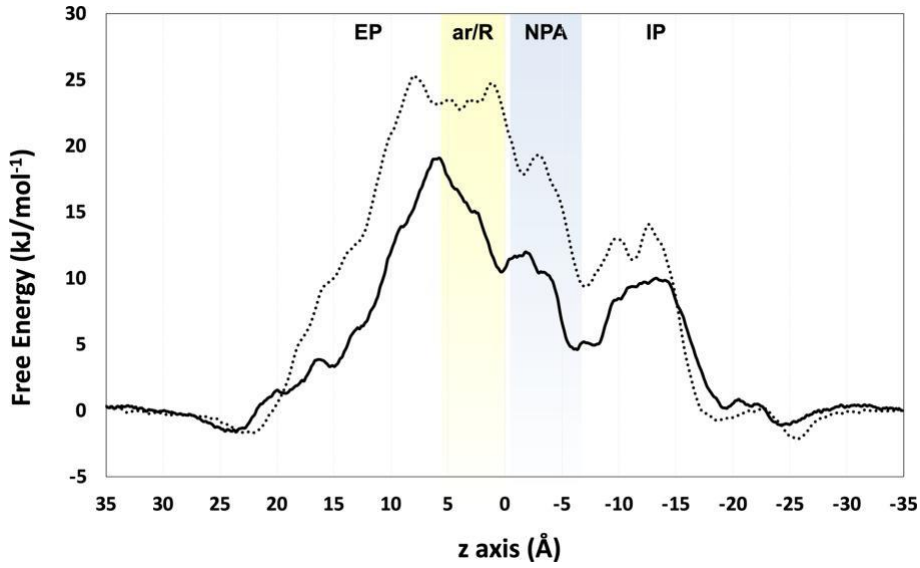

Fig. 4 Free energy (G) of glycerol uptake in WT hAQP10 (solid line) and hAQP10-$C^{CO}N$ adduct (dotted line). The data represents the averaged FES data from multiple successful permeation events calculated by metadynamics. Positions of ar/R SF and NPA motif are highlighted in yellow and blue, respectively.

the distance along the z-axis (Å) represented the selected CV. In total, seventeen 200 ns calculations were run for each system, for a total of 6.8 μs simulation time, which allowed for the obser-vation of multiple glycerol conductance events. Free-energy sur-faces were obtained for each glycerol molecule in both systems from successful single permeation events, which were averaged into a representative G (Fig. 4).

While the overall FES profiles are feature-consistent in both models, the hAQP10-$C^{CO}N$ adduct shows an average increase in free energy of ca. 7 kJ/mol compared to the WT form (WT = 20.71 kJ/mol and Cys arylated adduct = 27.47 kJ/mol, respectively) (Fig. 4). Both energy profiles display the highest increase in energy as glycerol enters the hAQP10 extracellular pocket (EP) ($z = 20$ to 7 Å) (Fig. 3), with the hAQP10-$C^{CO}N$ sys-tem showing a significantly higher top energy barrier ($10 < z < 0$), which is therefore the main signature of the presence of the compound (dotted line in Fig. 4). However, the influence of the compound extends well beyond local changes, affecting most of the free energy profile between $17 < z < -15$ Å. In fact, the free energy profile in the hAQP10-$C^{CO}N$ system remains consistently above the one of the WT system, at least until glycerol has passed through the NPA motif into the IP region, $z > -15$ Å.

Glycerol movement from the NPA towards the His80 gating re-gion (IP, $-15 < z < -7$ Å) is associated with an energy increase in both systems (ca. 5 kJ/mol) due to the narrowing and enhanced steric demand of the pore. Therein, the number of glycerol–amino acid residue interactions increases, while the number of glycerol– water H–bond interactions is reduced, between 2 and 5 interac-tions in bulk water, over 1 and 3 in the wider EP region of the chan-nel, and finally 0 to 2 waters in the most constricted IP region of the pore, on average.

From an overall analysis of the conformational differences be-tween the WT hAQP10 and hAQP10-$C^{CO}N$ models, important ef-fects on the pore size are induced by the postulated cysteine ary-lation. In details, the Hole 2 software[44] was used to measure the dimensions of each pore in a number of simulation snapshots for both WT and modified hAQP10, and evidenced shrinkage of various portions of the channel (Fig. 5A). In a typical WT hAQP10 conductance event, glycerol access to the EP of hAQP10 is unhin-dered in any orientation, which allows for maintenance of interac-tions with water. On approaching the ar/R SF, a more longitudinal

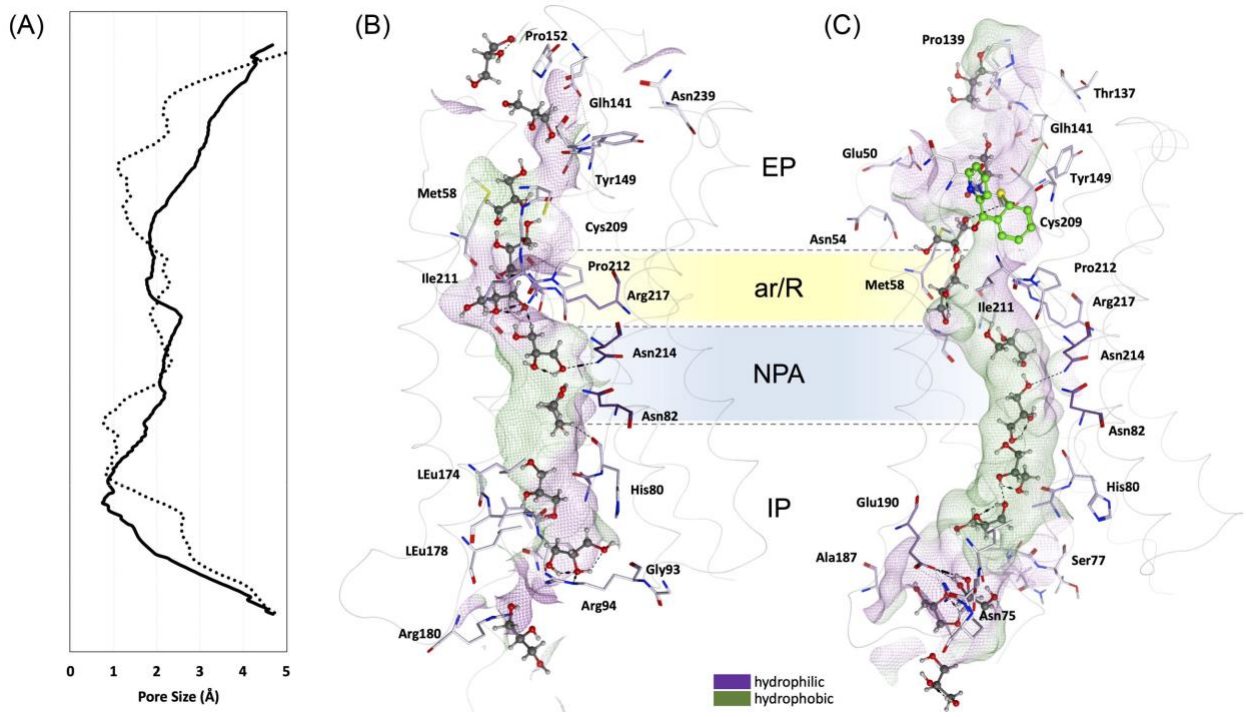

Fig. 5 (A) Pore size of WT hAQP10 (solid line) and hAQP10-C^{CO}N adduct (dotted line) as a 2D representation glycerol permeation routes for WT hAQP10 (B) and hAQP10-C^{CO}N (C) from metadynamics calculations. Multiple glycerol molecule snapshots are taken from one representative simulation from each system and overlaid to produce a single path. Key amino acids involved in conductance are explicitly shown and colour-mapped according to H-bond residence time (short = light, long = dark). Glycerol molecules are shown in VDW representation, key amino acids are shown in liquorice representation, and Cys209 + compounds are shown in ball and stick representation with the compound coloured green for clarity. Figure A was generated using HOLE data,[44] figures B and C were generated using MOE software.[43]

orientation is preferred. Due to the relatively wide nature of the hAQP10 channel, glycerol is still able to rotate throughout the pore and to establish interactions with residues within the pore as well as with water molecules (Fig. 5B). In contrast, in the hAQP10-C^{CO}N bound model, glycerol is hindered from rotating within the EP due to the reduced pore size, which enforces a longitudinal orienta-tion throughout (Fig. 5C). Moreover, the hindering of the glycerol rotation is maintained as it passes through the IP region around His80.

As it can be observed in Figs 5A and 6, pore shrinkage occurs upon arylation of Cys209, with an overall protein conformational change involving both the intracellular pore (IP) and EP. This re-sult, in conjunction with the increase in average free-energy for glycerol passage, may be taken as an explanation of the observed hAQP10 inhibitory effects of compound **2** in the functional as-says. Of note, the observed successful conductance events for glycerol uptake were reduced to 65%, in the arylated hAQP10 model with respect to the WT (82%), based on metadynamics results.

To further investigate the difference in glycerol conduction events between the two systems, their respective electrostatic sufaces were generated using the Adaptive Poisson-Boltzmann Solver (APBS)[46] (Fig. 7). An analysis of the extracellular pore en-trances shows overall positively charged surfaces in both cases, with the WT having a more extended positive surface charge than the C^{CO}N-bound hAQP10 model. As surface interactions within the EP are key to substrate approach and conductance, changes in this area further pinpoint the observed affinity differ-ences in glycerol uptake between WT and C^{CO}N-bound hAQP10. Changes to biological channel transport mechanisms due to elec-trostatics are well known and have been observed previously for other porins.[19, 47] It should also be noted that the markedly pos-itively charged surface of hAQP10 at pH 5.0 may be responsi-ble for the scarce affinity of the cationic compound **5** for pro-tein binding/inhibition, as evidenced in the functional assays; al-though, the same does not account for the cationic Auphen. In the case of **5**, the stability of the metformin chelating ligand could also disfavour ligand exchange reactions at the target cysteine site.

Noteworthy, in a previous study, the continuum Poisson– Boltzmann electrostatic potential along the pore was calcu-lated and compared for a number of AQPs isoforms, including some aquaglyceroporins.[48] Overall, the authors concluded that aquaglyceroporins show a rather flat potential all along the chan-nel, particularly at the ar/R SF, which may account for their sub-strate selectivity. In the case of the bacterial glycerol facilita-tor (GlpF), the electrostatic potential at the cytoplasmic entrance was calculated to be between 0 and−5 kT/e.[48] Our preliminary data show that at pH 5.0 (relevant to this specific AQP isoform), the electrostatic potential at the hAQP10 cytoplasmic entrance is around +10 to +12 kT/e, and it can reach negative values only at neutral pH.

To better understand the molecular pathway of glycerol pas-sage though the pores, the hydrogen bond analysis tool, avail-able in VMD,[45] was used to analyse the H-bond interactions, and respective residence times, between the protein and glyc-erol for every successful conductance event observed in both sys-tems (Fig. 8). In this case, a more or less pronounced presence of hydrogen bonds is a good description for a switch from solute– solvent (water) interactions to solute–protein (residue) interac-tions, which correlates with filter region energy demand and re-tention time.

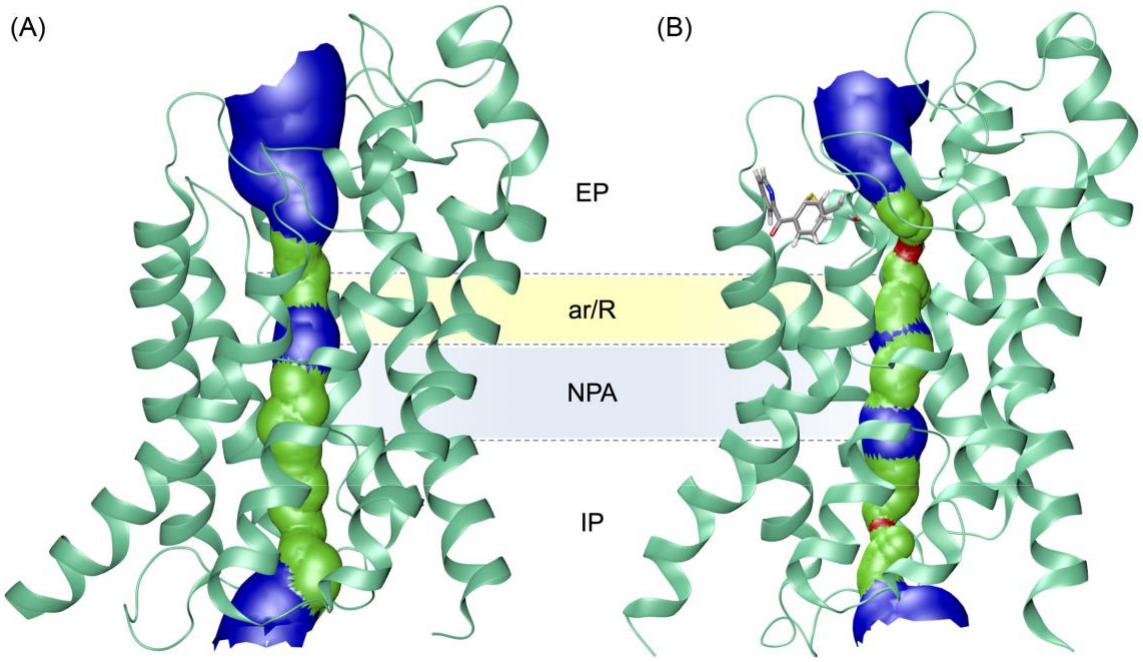

Fig. 6 Ribbon representation of the WT hAQP10 monomer (A) and of the hAQP10-C^{CO}N adduct with modified Cys209 (B), showing the effects of pore size as a 3D representation (based on VDW radius: red = smaller than single H_2O, green = single H_2O, blue = larger than single H_2O). Cys209-C^{CO}N fragment is shown in stick representation with atoms coloured by atom type. Figure generated using HOLE[44] and VMD software.[45]

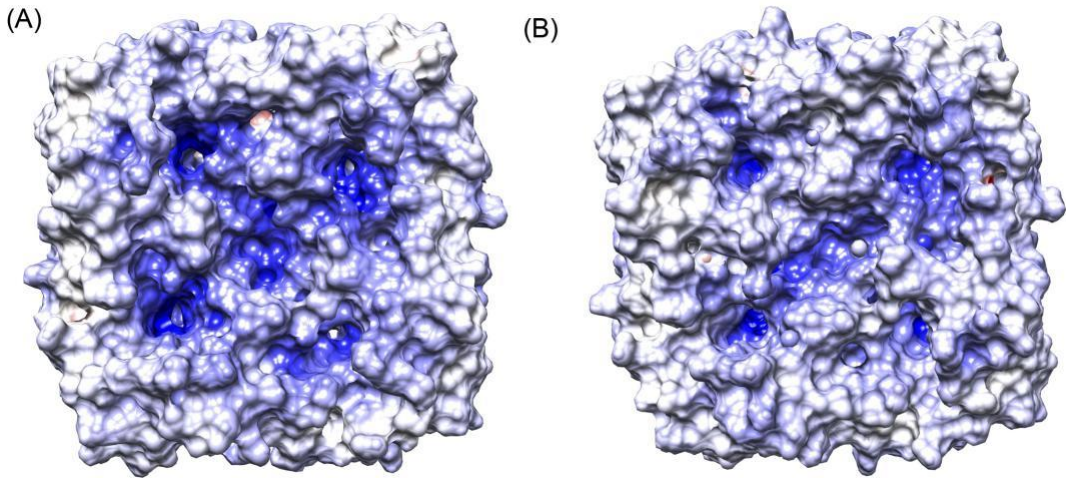

Fig. 7 Extracellular electrostatic surfaces of WT hAQP10 (A) and hAQP10-C^{CO}N (B) with the following colour code: positively charged = blue, negatively charged = red, neutral = white. Surfaces were generated using the Adaptive Poisson-Boltzmann Solver (APBS)[46] and rendered using Chimera software.[49]

In the WT hAQP10, hydrogen bond data confirm the involve-ment of the residues of the ar/R SF and NPA motif in glycerol flux, with the addition of residue Thr38 in the ar/R SF (Figs 5 and 8). However, upon covalent binding of the C^{CO}N ligand, the pathway of glycerol conductance is markedly altered and a number of new residues in the EP becomes more involved, namely Thr51, Lys52, Asn54, and Asn208, principally due to the increased protrusion of the loop into the pore. Moreover, cysteine arylation appears to change the conformation of the protein by extending the constric-tion of the hAQP10 pore from the pH gating region towards the NPA motif (Fig. 5A). The data show no increase in H-bond resi-dence time in this area, causing no increased rigidity of the protein, thus, still allowing solute passage. The key residues of the IP region involved in glycerol conductance, identified in both the WT and C^{CO}N-hAQP10 systems, are Asn75, Val76, Ser77, Ala79, His80, and Arg94, respectively. This is in agreement with the residues found experimentally to be responsible for the pH gating mecha-nism.[10]

To address the effects of the compound's binding on water per-meation representative conductance simulations for both WT and hAQP10-C^{CO}N were performed. The obtained results revealed that water conductance is temporarily halted in at least one of the adjacent pores of the tetramer as glycerol reaches the most con-stricted region of the pore (around the His90 located in the IP) (see

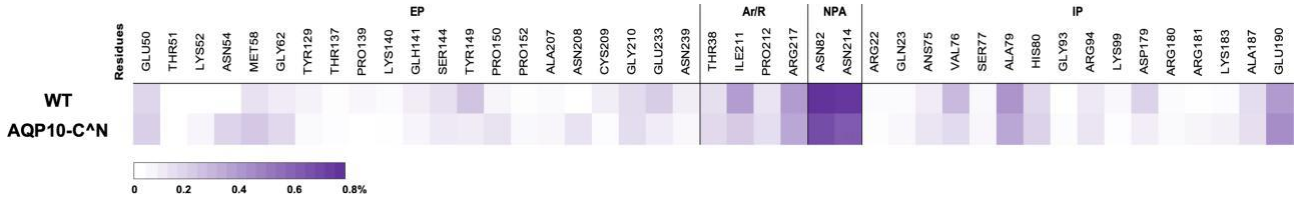

Fig. 8 Averaged glycerol H-bond residence time based on metadynamics simulations of WT hAQP10 vs hAQP10-C^{CO}N adduct, with key amino acids involved in conductance colour-mapped according to residence time in % of time of trajectory spent H-bonding.

movies AQP10_C(co)N.mp4 and AQP10_WT.mp4). The local distor-tion within a channel, caused by large solute molecules like glyc-erol, maps onto adjacent pores in the form of protein conforma-tional changes, which are pronounced enough to impede further water mobility until the glycerol has exited the constricted region.

A further consideration concerns the observed similarity of glycerol permeation through AQP10 and AQP3. Specifically, our metadynamics simulations evidenced that in both isoforms, wa-ter plays a pivotal role as a conductance facilitator. In AQP3, glyc-erol takes advantage of the water chain passing through the pore, as it opportunistically plugs itself into the single-file water chain, a dynamic chain that is only episodically disrupted in the most sterically constricted ar/R region of the pore in the case of AQP3 and the IP region of AQP10, with the glycerol–water chain be-ing promptly re-established after negotiating the steric narrow-ing. Water movement via AQP10, under equilibrium conditions, was found to match what was previously reported for AQP3,[36,37] in particular the remarkable bi-directional water permeation and the ability for water molecules to 'hop' over each other in order to maintain this bi-directionality. This has now been observed for both hAQP10 WT and hAQP10-C^{CO}N bound systems, which fur-ther consolidates the fundamental dynamic roles of this mecha-nism, prior to any guest molecule shuffling.

Conclusions

In light of the broad range of functions of AQPs in physiology and disease mechanisms, the development of their selective inhibitors is pivotal, as these could be used as either chemical probes to detect the proteins' function in biological systems, or as novel therapeutic agents in a variety of disease states. Here, we report on the potent and irreversible inhibition of glycerol permeation via human AQP10 by a family of organogold compounds stud-ied in an optimized *S. cerevisiae* model by fluorescence stopped-flow. At variance with the benchmark inhibitor Auphen, the Au(III) C^N compounds are known to easily react with cysteine residues in proteins via a mechanism whereby first a gold coordination adduct occurs at a Cys residue (Au–S bond formation), followed by the metal-templated transfer of the C^N ligand to the thiol of the aforementioned cysteine (C–S bond formation).

Amongst the selected series, compound **2** resulted to be one of the most active to inhibit glycerol permeation in hAQP10 overexpressing cells. Functional assays in the presence of β-mercaptoethanol demonstrated the irreversible inhibition of hAQP10 glycerol permeability by **2**, in line with the expected co-valent modification of cysteine residues in the pore. Initial mech-anistic insights on the effects of the inhibitors' binding to hAQP10 were obtained by metadynamics. Specifically, upon covalent bind-ing of the C^{CO}N ligand to Cys209, the pathway of glycerol con-ductance is significantly altered and an overall shrinkage of the pore is observed, while water flux is minimally affected. Therein, the whole pore responds to an otherwise only local change in the internal pore structure. Even if the arylation is taking place at a distance from the highly conserved ar/R SF and NPA regions, it increases the free energy profile height globally, i.e. almost over the entire pore length. This indicates that pore dynamics over the timescale of translocations events are as important factors in modulating small molecule translocation as are specific filtering regions. Further metadynamics studies including a direct imple-mentation of the osmotic flux through AQP10 in large scale simu-lations are warranted in order to fully assess the effect of cysteine arylation on substrate permeability.

Experimental section

General

Solvents and reagents (reagent grade) were all commercially avail-able and used without further purification. Compounds **1–5** and Auphen were synthesized adapting procedures already reported in literature,[24–28,38] and their purity confirmed by elemental anal-ysis (>98%).

Cloning and heterologous expression of hAQP10 in *S. cerevisiae*

The **hAQP10** expression plasmid was based on a yeast codon optimized cDNA sequence (Genscript, USA) and constructed by homologous recombination in yeast strain YSH1770 by co-transformation of a hAQP10 derived PCR fragment and *Bam*HI, *Sal*I, *Hin*dIII digested pUG35 as described before.[10] The trans-formed YSH1770 yeast strain produces the native hAQP10 primary structure without any tags.

Yeast strains and growth conditions

Yeast cultures were grown at 28°C with orbital shaking in yeast ni-trogen base (YNB) without amino acids (DIFCO), with 2% (wt/vol) glucose and supplemented with the adequate requirements for prototrophic growth.[50] Transformants were grown to $OD_{600nm} \approx 1$ (corresponding to 1×10^7 cells ml^{-1}), harvested by centrifugation (5 000 × g, 10 min, 4°C), washed three times and re-suspended in ice-cold sorbitol (sorbitol 1.4 M in 50 mM K^+-citrate buffer pH 5.0) up to a concentration of 0.33 g (wet weight) ml^{-1}, and kept on ice for at least 90 min. Prior to osmotic challenges, cells were preloaded with the nonfluorescent precursor 5-and-6-carboxyfluorescein diacetate (CFDA, Sigma, USA; 1 mM for 20 min at 30°C) that is cleaved intracellularly by nonspecific esterases to generate the membrane impermeable fluorescent form car-boxyfluorescein (CF) known to remain in the cytoplasm.[51] Cells were then diluted 1:10 in 1.4 M sorbitol buffer and immediately used for stopped-flow experiments.

Permeability assays

Stopped-flow fluorescence spectroscopy was used to monitor cell volume changes of yeast transformants loaded with the

concentration-dependent self-quenching fluorophore CFDA as described above.[51] Experiments were performed on a HI-TECH Scientific PQ/SF-53 stopped-flow apparatus, with 2 ms dead time and controlled temperature, interfaced with an IBM PC/AT com-patible 80 386 microcomputer. The cells were challenged with an equal volume of shock solution at 23°C and the time course of volume change was measured by following the fluorescence in-tensity (excitation 470 nm and emission 530 nm). For each exper-imental condition, 5–7 replicates were analysed. Baselines were acquired using the incubation buffers as isotonic shock solutions. For glycerol permeability (P_{gly}) measurements, a hyperosmotic so-lution containing glycerol (glycerol 2.1 M in 50 mM K^+ -citrate pH 5.0) was used to create an inwardly directed glycerol gradient.[52,53] After the first fast cell shrinkage due to water outflow, glycerol influx in response to its chemical gradient is followed by water influx and cell re-swelling. Fluorescent traces were corrected by subtracting the baseline slope that reflects the bleaching of the fluorophore. The calibration of the resulting traces followed our previous strategy.[52] Evaluation of P_{gly} was achieved by numer-ical integrations using a mathematical model implemented in the Berkeley Madonna software (http://www.berkeleymadonna. com/) as described.[19] To assess the effect of the gold compounds, Auphen and the five cyclometalated Au(III) complexes, cells were incubated with compounds for 30 min at RT before stopped-flow experiments.

The reversibility of P_{gly} inhibition was evaluated by pre-treating hAQP10-expressing yeast cells with 10 μM of compound 2 or Auphen and subsequently washing with isotonic buffer or with the reducing agent βME prior to permeability assays. Briefly, cells were centrifuged (5 000 × g, 10 min), washed twice with isotonic buffer or with βME (100 μM), and then re-suspended in isotonic buffer prior to permeability assays. Non-pre-treated cells were also washed with βME and used as control.

Statistical analysis

The results were expressed as mean ± SD of three individual ex-periments. Data were first analysed with Shapiro–Wilk normal-ity test to assure a normal distribution, followed by unpaired Student's t-test using the Prism software (GraphPad Software Inc., San Diego, CA). P values <0.05 were considered statistically significant.

Computational studies

Two hAQP10 models were built using the XRD-derived crystal structure of hAQP10 (PDB-ID 6F7H),[10] one WT and one with the $C^{CO}N$ ligand covalently bound to the sulfur of Cys209 in each monomer. The parameters for the compound bound to Cys209 and for the glycerol model were generated by the Automated Topology Builder and Repository (ATB, version 2.2) website using the B3LYP/6-31G* basis set, using a combination of semi-empirical quantum mechanics (QM) and DFT.[54] The models were proto-nated to pH 5 using the PDB2PQR server[42] to mimic the physio-logical conditions. Each simulation box (10 × 10 × 15 nm in size) contained the hAQP10 tetramer inserted into a lipid bilayer, con-stituted by 203 POPE lipids (carried out using the charm GUI online server[55,56]. Each system was solvated with TIP3P water molecules, with the number added being dependent on the system. For the WT, 33 327 water molecules were added; while for the system with the compound bound, the number of water molecules was 33 351. Periodic boundary conditions (PBCs) were used for each system. Thirty chloride ions were substituted for corresponding water molecules to neutralise the charges of each system. An adapted Amber14SB_OL15 + lipids force field[57] was used for all the simulations, with the addition of the parameters for the com-pound bound cystine residue.

All simulations were run using the GROMACS 2020.2 soft-ware.[58] The particle-mesh Ewald method was used for calculating long-range electrostatic interactions, the Verlet cut-off scheme, with a cut-off distance of 0.8 nm, was used for short-range re-pulsive and attractive interactions, and Lincs used to constrain all bond lengths. Nose–Hoover[59] temperature coupling was used to maintain the temperature of the system (τ = 0.5 ps) at 300 K, while the Parrinello-Rahman[60] algorithm was used to maintain the pressure of the system at 1 bar with a coupling constant of τ = 1.0 ps. Simulations were equilibrated for 100 ps before production.

Metadynamics simulations

Well-tempered metadynamics simulations were run for 200 000 000 steps with a 1 fs time-step (200 ns) using the Plumed plugin[34] for GROMACS. The distance CV was used be-tween the COM of glycerol molecules and a plane formed by the backbone carbons of Asparagine 214 from each of the four monomers. This provided a reference plane in the centre of the system, equating to the top of the NPA motif. Each of the 20 glycerol molecules was given a separate plumed control within the same data file, allowing the free-energy for each molecule to be calculated within each simulation. Gaussians were added every 2000 steps (2 ps), giving a deposition rate of 0.025 kJ/mol.ps. Gaussian height was 50 TAU and the Gaussian width was 0.25 A˚. The bias factor was set to 12, T was 3600 K.

Free-energy surface data were normalised by setting the base-line to 0 and excluding bulk water on either side of the pore. Free-energy surface data was taken from the trajectories in which glyc-erol molecule passed through a pore, in either direction, once dur-ing the simulation; and molecules re-crossing the pore or passing through the lipid membrane were excluded. This resulted in 56 FES for the WT system (46 for uptake and 10 for efflux) and 54 FES for the compound bound system (35 for uptake and 19 for efflux), which were used for calculating G values (KJ/mol).

Acknowledgements

B.A. acknowledges the EU Erasmus Program for supporting a short-term scientific mission at the Universidade de Lisboa. The authors gratefully acknowledge the support of NVIDIA Corpora-tion with the donation of a Quadro P5000 GPU used for this re-search. The authors thank ARCCA for access to computational facilities. The authors gratefully acknowledge the Gauss Centre for Supercomputing e.V. (www.gauss-centre.eu) for funding this project by providing computing time on the GCS Supercomputer SuperMUC at Leibniz Supercomputing Centre (www.lrz.de).

Funding

The authors acknowledge FCT—Fundação para a Ciência e Tecnologia, grant PTDC/BTM-SAL/28977/2017, fellowship 2020.04974.BD to C. Pimpão and projects UIDB/04138/2020 and UIDP/04138/2020 to iMed.ULisboa.

Conflict of interest

Authors have no conflict of interest to declare.

Data availability

The data underlying this article will be shared on reasonable request to the corresponding author.

References

1. A. S. Verkman, Mammalian aquaporins: diverse physiological roles and potential clinical significance, *Expert Rev. Mol. Med.*, 2008, 10, 1–18.
2. I. V. da Silva, J. S. Rodrigues, I. Rebelo, J. P. G. Miranda and G. Soveral, Revisiting the metabolic syndrome: the emerging role of aquaglyceroporins, *Cell. Mol. Life Sci.*, 2018, 75 (11), 1973–1988.
3. I. V. da Silva and G. Soveral, Aquaporins in immune cells and inflammation: new targets for drug development, *Int. J. Mol. Sci.*, 2021, 22 (4), 1845.
4. G. Calamita, J. Perret and C. Delporte, Aquaglyceroporins: drug targets for metabolic diseases?, *Front. Physiol.*, 2018, 9, 851.
5. A. S. Verkman, M. O. Anderson and M. C. Papadopoulos, Aquaporins: important but elusive drug targets, *Nat. Rev. Drug Discovery*, 2014, 13 (4), 259–277.
6. S. Hatakeyama, Y. Yoshida, T. Tani, Y. Koyama, K. Nihei, K. Ohshiro, J. I. Kamiie, E. Yaoita, T. Suda, K. Hatakeyama and T. Yamamoto, Cloning of a new aquaporin (AQP10) abundantly expressed in duodenum and jejunum, *Biochem. Biophys. Res. Commun.*, 2001, 287 (4), 814–819.
7. K. Ishibashi, T. Morinaga, M. Kuwahara, S. Sasaki and M. Imai, Cloning and identification of a new member of water channel (AQP10) as an aquaglyceroporin, *Biochim. Biophys. Acta*, 2002, 1576 (3), 335–340.
8. U. Laforenza, E. Miceli, G. Gastaldi, M. F. Scaffino, U. Ventura, J. M. Fontana, M. N. Orsenigo and G. R. Corazza, Solute transporters and aquaporins are impaired in celiac disease, *Biol. Cell*, 2010, 102 (8), 457–467.
9. U. Laforenza, M. F. Scaffino and G. Gastaldi, Aquaporin-10 represents an alternative pathway for glycerol efflux from human adipocytes, *PLoS One*, 2013, 8 (1), e54474.
10. K. Gotfryd, A. F. Mósca, J. W. Missel, S. F. Truelsen, K. Wang, M. Spulber, S. Krabbe, C. Hélix-Nielsen, U. Laforenza, G. Soveral, P. A. Pedersen and P. Gourdon, Human adipose glycerol flux is regulated by a pH gate in AQP10, *Nat. Commun.*, 2018, 9 (1), 1–11.
11. H. Sui, B. G. Han, J. K. Lee, P. Walian and B. K. Jap, Structural basis of water-specific transport through the AQP1 water channel, *Nature*, 2001, 414 (6866), 872–878.
12. K. Murata, K. Mitsuoka, T. Hiral, T. Walz, P. Agre, J. B. Heymann, A. Engel and Y. Fujiyoshi, Structural determinants of water permeation through aquaporin-1, *Nature*, 2000, 407 (6804), 599–605.
13. D. Fu, A. Libson, L. J. W. Miercke, C. Weitzman, P. Nollert, J. Krucinski and R. M. Stroud, Structure of a glycerol-conducting channel and the basis for its selectivity, *Science*, 2000, 290 (5491), 481–486.
14. D. Wree, B. Wu, T. Zeuthen and E. Beitz, Requirement for asparagine in the aquaporin NPA sequence signature motifs for cation exclusion, *FEBS J.*, 2011, 278 (5), 740–748.
15. G. Soveral and A. Casini, Aquaporin modulators: a patent review (2010–2015), *Expert Opin. Ther. Pat.*, 2017, 27 (1), 49–62.
16. A. De Almeida, G. Soveral and A. Casini, Gold compounds as aquaporin inhibitors: new opportunities for therapy and imaging, *Med. Chem. Commun.*, 2014, 5 (10), 1444–1453.
17. A. P. Martins, A. Marrone, A. Ciancetta, A. Galán Cobo, M. Echevarría, T. F. Moura, N. Re, A. Casini and G. Soveral, Targeting aquaporin function: potent inhibition of aquaglyceroporin-3 by a gold-based compound, *PLoS One*, 2012, 7 (5), e37435.
18. A. Madeira, A. de Almeida, C. de Graaf, M. Camps, A. Zorzano, T. F. Moura, A. Casini and G. Soveral, A gold coordination compound as a chemical probe to unravel aquaporin-7 function, *ChemBioChem*, 2014, 15 (10), 1487–1494.
19. A. Mósca, A. de Almeida, D. Wragg, A. Martins, F. Sabir, S. Leoni, T. Moura, C. Prista, A. Casini and G. Soveral, Molecular basis of Aquaporin-7 permeability regulation by pH, *Cells*, 2018, 7 (11), 207.
20. A. P. Martins, A. Ciancetta, A. deAlmeida, A. Marrone, N. Re, G. Soveral and A. Casini, Aquaporin inhibition by gold(III) compounds: new insights, *ChemMedChem*, 2013, 8 (7), 1086–1092.
21. A. Serna, A. Galán-Cobo, C. Rodrigues, I. Sánchez-Gomar, J. J. Toledo-Aral, T. F. Moura, A. Casini, G. Soveral and M. Echevarría, Functional inhibition of aquaporin-3 with a gold-based compound induces blockage of cell proliferation, *J. Cell. Physiol.*, 2014, 229 (11), 1787–1801.
22. A. De Almeida, A. F. Mósca, D. Wragg, M. Wenzel, P. Kavanagh, G. Barone, S. Leoni, G. Soveral and A. Casini, The mechanism of aquaporin inhibition by gold compounds elucidated by biophysical and computational methods, *Chem. Commun.*, 2017, 53 (27), 3830–3833.
23. Y. Sonntag, P. Gena, A. Maggio, T. Singh, I. Artner, M. K. Oklinski, U. Johanson, P. Kjellbom, J. D. Nieland, S. Nielsen, G. Calamita and M. Rützler, Identification and characterization of potent and selective aquaporin-3 and aquaporin-7 inhibitors, *J. Biol. Chem.*, 2019, 294 (18), 7377–7387.
24. M. A. Cinellu, A. Zucca, S. Stoccoro, G. Minghetti, M. Manassero and M. Sansoni, Synthesis and characterization of gold(III) adducts and cyclometallated derivatives with 2-substituted pyridines. Crystal structure of [Au{NC5H4(CMe2C6H 4)-2}Cl2], *J. Chem. Soc. Dalton Trans.*, 1995, 1 (17), 2865–2872.
25. Y. Fuchita, H. Ieda, Y. Tsunemune, J. Kinoshita-Nagaoka and H. Kawano, Synthesis, structure and reactivity of a new six-membered cycloaurated complex of 2-benzoylpyridine [AuCl2(pcp-C1,N)] [pcp = 2-(2-pyridylcarbonyl)phenyl]. Comparison with the cycloaurated complex derived from 2-benzylpyridine, *J. Chem. Soc. Dalton Trans.*, 1998, 2 (5), 791–796.
26. M. A. Cinellu, A. Zucca, S. Stoccoro, G. Minghetti, M. Manassero and M. Sansoni, Synthesis and characterization of gold(III) adducts and cyclometallated derivatives with 6-benzyl- and 6-alkyl-2,2 -bipyridines, *J. Chem. Soc. Dalton Trans.*, 1996(22), 4217–4225.
27. K. K. Y. Kung, H. M. Ko, J. F. Cui, H. C. Chong, Y. C. Leung and M. K. Wong, Cyclometalated gold(iii) complexes for chemoselective cysteine modification via ligand controlled C—S bond-forming reductive elimination, *Chem. Commun.*, 2014, 50 (80), 11899–11902.
28. M. V. Babak, K. R. Chong, P. Rapta, M. Zannikou, H. M. Tang, L. Reichert, M. R. Chang, V. Kushnarev, P. Heffeter, S. M. Meier-Menches, Z. C. Lim, J. Y. Yap, A. Casini, I. V. Balyasnikova and W. H. Ang, Interfering with metabolic profile of triple-negative breast cancer using rationally-designed metformin prodrugs, *Angew. Chemie Int. Ed.*, 2021, 60 (24), 13405–13413.
29. C. Rodrigues, C. Pimpão, A. F. Mósca, A. S. Coxixo, D. Lopes, I. V. Da Silva, P. A. Pedersen, F. Antunes and G. Soveral, Human aquaporin-5 facilitates hydrogen peroxide permeation affecting adaption to oxidative stress and cancer cell migration, *Cancers*, 2019, 11 (7), 932.
30. C. Pimpão, I. V. da Silva, A. F. Mósca, J. O. Pinho, M. M. Gaspar, N. I. Gumerova, A. Rompel, M. Aureliano and G. Soveral, The aquaporin-3-inhibiting potential of polyoxotungstates, *Int. J. Mol. Sci.*, 2020, 21 (7), 2467.

31. M. N. Wenzel, R. Bonsignore, S. R. Thomas, D. Bourissou, G. Barone and A. Casini, Cyclometalated AuIII complexes for cysteine ary-lation in zinc finger protein domains: towards controlled reduc-tive elimination, *Chemistry*, 2019, 25 (32), 7628–7634.
32. S. R. Thomas, R. Bonsignore, J. Sánchez Escudero, S. M. Meier-Menches, C. M. Brown, M. O. Wolf, G. Barone, L. Y. P. Luk and A. Casini, Exploring the chemoselectivity towards cysteine aryla-tion by Cyclometallated AuIII compounds: new mechanistic in-sights, *ChemBioChem*, 2020, 21 (21), 3071–3076.
33. S. R. Thomas and A. Casini, Gold compounds for catalysis and metal-mediated transformations in biological systems, *Curr. Opin. Chem. Biol.*, 2020, 55, 103–110.
34. G. A. Tribello, M. Bonomi, D. Branduardi, C. Camilloni and G. Bussi, PLUMED 2: new feathers for an old bird, *Comput. Phys. Com-mun.*, 2014, 185 (2), 604–613.
35. D. Wragg, A. de Almeida, R. Bonsignore, F. E. Kühn, S. Leoni and A. Casini, On the mechanism of Gold/NHC compounds binding to DNA G-quadruplexes: combined metadynamics and biophysical methods, *Angew. Chem. Int. Ed.*, 2018, 57 (44), 14524–14528.
36. D. Wragg, A. de Almeida, A. Casini and S. Leoni, Unveiling the mechanisms of aquaglyceroporin-3 water and glycerol perme-ation by metadynamics, *Chemistry*, 2019, 25, 8713–8718.
37. D. Wragg, S. Leoni and A. Casini, Aquaporin-driven hydrogen per-oxide transport: a case of molecular mimicry?, *RSC Chem. Biol.*, 2020, 1 (5), 390–394.
38. B. P. Block and J. C. Bailar, The reaction of Gold (III) with some bidentate coördinating groups, *J. Am. Chem. Soc.*, 1951, 73 (10), 4722–4725.
39. G. F. Sprague and J. E. Cronan, Isolation and characteriza-tion of Saccharomyces cerevisiae mutants defective in glycerol catabolism, *J. Bacteriol.*, 1977, 129 (3), 1335–1342.
40. E. Campos, T. F. Moura, A. Oliva, P. Leandro and G. Soveral, Lack of Aquaporin 3 in bovine erythrocyte membranes correlates with low glycerol permeation, *Biochem. Biophys. Res. Commun.*, 2011, 408 (3), 477–481.
41. A. Casini, A. Guerri, C. Gabbiani and L. Messori, Biophysical char-acterisation of adducts formed between anticancer metallo-drugs and selected proteins: new insights from X-ray diffraction and mass spectrometry studies, *J. Inorg. Biochem.*, 2008, 102 (5-6), 995–1006.
42. T. J. Dolinsky, J. E. Nielsen, J. A. McCammon and N. A. Baker, PDB2PQR: an automated pipeline for the setup of Poisson-Boltzmann electrostatics calculations, *Nucleic Acids Res.*, 2004, 32 (Web Server), W665–W667.
43. Chemical 931 Computing Group, Molecular Operating Environ-ment, 2020. ver. 2019.01. ULC Montreal, Canada, 2020.
44. O. S. Smart, J. G. Neduvelil, X. Wang, B. A. Wallace and M. S. P. Sansom, HOLE: a program for the analysis of the pore dimen-sions of ion channel structural models, *J. Mol. Graph.*, 1996, 14 (6), 354–360.
45. W. Humphrey, A. Dalke and K. Schulten, VMD: visual molecular dynamics, *J. Mol. Graph.*, 1996, 14 (1), 33–38.
46. N. A. Baker, D. Sept, S. Joseph, M. J. Holst and J. A. McCam-mon, Electrostatics of nanosystems: application to microtubules and the ribosome, *Proc. Natl. Acad. Sci.*, 2001, 98 (18), 10037– 10041.
47. H. Bajaj, M. A. Scorciapino, L. Moynie, M. G. P. Page, J. H. Naismith, M. Ceccarelli and M. Winterhalter, Molecular basis of filtering carbapenems by porins from βlactam-resistant clinical strains of Escherichia coli, *J. Biol. Chem.*, 2016, 291 (6), 2837–2847.
48. R. Oliva, G. Calamita, J. M. Thornton and M. Pellegrini-Calace, Electrostatics of aquaporin and aquaglyceroporin channels cor-relates with their transport selectivity, *Proc. Natl. Acad. Sci.*, 2010, 107 (9), 4135–4140.
49. E. F. Pettersen, T. D. Goddard, C. C. Huang, G. S. Couch, D. M. Green-blatt, E. C. Meng and T. E. Ferrin, UCSF Chimera - a visualization system for exploratory research and analysis, *J. Comput. Chem.*, 2004, 25 (13), 1605–1612.
50. J. T. Pronk, Auxotrophic yeast strains in fundamental and applied research, *Appl. Environ. Microbiol.*, 2002, 68 (5), 2095–2100.
51. G. Soveral, A. Madeira, M. C. Loureiro-Dias and T. F. Moura, Water transport in intact yeast cells as assessed by fluores-cence self-quenching, *Appl. Environ. Microbiol.*, 2007, 73 (7), 2341– 2343.
52. G. Soveral, A. Madeira, M. C. Loureiro-Dias and T. F. Moura, Mem-brane tension regulates water transport in yeast, *Biochim. Bio-phys. Acta*, 2008, 1778 (11), 2573–2579.
53. A. De Almeida, A. P. Martins, A. F. Mósca, H. J. Wijma, C. Prista, G. Soveral and A. Casini, Exploring the gating mechanisms of aquaporin-3: new clues for the design of inhibitors?, *Mol. Biosyst.*, 2016, 12 (5), 1564–1573.
54. A. K. Malde, L. Zuo, M. Breeze, M. Stroet, D. Poger, P. C. Nair, C. Oostenbrink and A. E. Mark, An automated force field topology builder (ATB) and repository: version 1.0, *J. Chem. Theory Comput.*, 2011, 7 (12), 4026–4037.
55. S. Jo, T. Kim, V. G. Iyer and W. Im, CHARMM-GUI: a web-based graphical user interface for CHARMM, *J. Comput. Chem.*, 2008, 29 (11), 1859–1865.
56. E. L. Wu, X. Cheng, S. Jo, H. Rui, K. C. Song, E. M. Dávila-Contreras, Y. Qi, J. Lee, V. Monje-Galvan, R. M. Venable, J. B. Klauda and W. Im, CHARMM-GUI Membrane Builder toward realistic biologi-cal membrane simulations, *J. Comput. Chem.* 2014, 35 (27), 1997– 2004.
57. C. Tian, K. Kasavajhala, K. A. A. Belfon, L. Raguette, H. Huang, A. N. Migues, J. Bickel, Y. Wang, J. Pincay, Q. Wu and C. Simmer-ling, Ff19SB: amino-acid-specific protein backbone parameters trained against quantum mechanics energy surfaces in solution, *J. Chem. Theory Comput.*, 2020, 16 (1), 528–552.
58. A. Lindahl and H. van der Spoel, GROMACS 2020. 2 Manual, 2020.
59. S. Nosé, A molecular dynamics method for simulations in the canonical ensemble, *Mol. Phys.*, 1984, 52 (2), 255–268.
60. M. Parrinello and A. Rahman, Crystal structure and pair poten-tials: a molecular-dynamics study, *Phys. Rev. Lett.*, 1980, 45 (14), 1196–1199.